Available online at www.sciencedirect.com
SCIENCE DIRECT
Tectonophysics 413 (2006) 249–269
TECTONOPHYSICS
www.elsevier.com/locate/tecto

2-D seismic tomographic and ray tracing modelling of the crustal structure across the Sudetes Mountains basing on SUDETES 2003 experiment data

Mariusz Majdański [a,*], Marek Grad [a], Aleksander Guterch [b], SUDETES 2003 Working Group[1]

[a] *Institute of Geophysics, University of Warsaw, Pasteura 7, 02-093 Warsaw, Poland*
[b] *Institute of Geophysics, Polish Academy of Sciences, Ks. Janusza 64, 01-452 Warsaw, Poland*

Received 12 May 2005; received in revised form 19 September 2005; accepted 24 October 2005
Available online 3 January 2006

Abstract

The seismic data obtained during SUDETES 2003 experiment are analysed, and detailed crustal structure for profiles S02, S03 and S06 is presented using three different 2-D techniques: (1) "smooth" tomography of refracted waves travel times, (2) ray tracing of reflected and refracted waves, and (3) joint velocity and depth of reflector tomographic inversion. In spite of different interpretation techniques used, the models of the crustal structure show common characteristic features. The low velocity (V_p<4 km/s) sedimentary layer was documented in the northeastern part of the study area. The topmost basement has in general a velocity of 5.8–6.0 km/s, and velocities at ca. 20 km depth are 6.15–6.25 km/s. The strong reflecting boundaries were found at 20–23 and 25–28 km depth with a velocity contrast about 0.4 km/s, and the highest velocities in the lowermost crust are 6.8–7.2 km/s. In general, the crust of the Bohemian Massif is slightly thicker (33–35 km) than in the northern part of the area. Velocities beneath Moho are relatively low, of 7.95 km/s. On the basis of well recorded reflected waves, mantle reflectors were discovered in the depth interval ca. 40–70 km. Apart of new results for the geology and tectonics of the area, some conclusion could be made about different techniques used. In the 2-D case the "clasical" ray tracing method with using all correlated phases gives the most adequate model of the structure, because of full, manual control of the model creation. The "smooth" first arrival travel times tomography, although very fast, is not satisfactory enough to describe the complex structure. So, the best candidate in 3-D case seems to be travel time tomography for both refracted and reflected waves in multi-layers models.

Keywords: Crustal structure; Seismic ray-tracing; Travel time tomography; SUDETES 2003

[1] M. Behm, T. Bodoky, R. Brinkmann, M. Brož, E. Brueckl, W. Czuba, T. Fancsik, B. Forkmann, M. Fort, E. Gaczyński, W.H. Geissler, M. Grad, R. Greschke, A. Guterch, S. Harder, E. Hegedűs, A. Hemmann, P. Hrubcová, T. Janik, G. Jentzsch, G. Kaip, G.R. Keller, K. Komminaho, M. Korn, O. Korousová, M. Majdański, J. Málek, M. Malinowski, K.C. Miller, E.-M. Rumpfhuber, A. Špičák, P. Środa, E. Takács, T. Tiira, J. Vozár, M. Wilde-Piórko, J. Yliniemi, A. Żelaźniewicz.

* Corresponding author. Fax: +48 22 8222387.
E-mail address: mmajd@igf.fuw.edu.pl (M. Majdański).

0040-1951/$ - see front matter © 2005 Elsevier B.V. All rights reserved.
doi:10.1016/j.tecto.2005.10.042

1. Introduction and the geology of the area

SUDETES 2003 experiment (Grad et al., 2003b; Fig. 1) is the fourth from a series of large seismic experiments performed in 1997–2003 in Central Europe between Baltic and Adriatic seas, and it covers the gap between areas of POLONAISE'97, CELEBRATION 2000 and ALP 2002 experiments (Guterch et al., 1998, 1999, 2001, 2003a,b; Brueckl et al., 2003). The primary scientific goal of these experiments was to investigate the deep structure of the southwestern margin of the East European craton (EEC) and its relation to accreted younger terranes in the south (TESZ). The Palaeozoic accretion (amalgamation) of this area was in three stages: (1) Cambrian accretion of the Bruno–Silesian, Łysogóry and Małopolska terranes, (2) End Ordovician/Early Silurian accretion of Avalonia, and (3) Early Carboniferous accretion of Armorica (Winchester and the PACE TMR Network Team, 2002). Armorica, more recently termed the Armorican Terrane Assemblage (ATA; e.g., Franke, 2000; Tait et al., 2000; Winchester et al., 2002), extends across Europe from southern Spain to the Carpathian Mountains for around 4000 km in length and locally up to 700 km in width (Paris and Robardet, 1990). Apart of Iberia and French Massif Central, the Bohemian Massif is the largest stable outcrop of pre-Permian rocks in Western Europe (about 90,000 km^2), and it forms the easternmost rim of the Variscan Belt (Matte et al., 1990; Pin, 1990). In the past, the Bohemian Massif has been subdivided into various zones (Saxoturingian, Moldanubian, Moravian, Sudetes, etc.), and recently many authors propose new subdivisions of the Bohemian Massif and surroundings (e.g., Cymerman et al., 1997; Żelaźniewicz, 1997; Unrug et al., 1999; Franke and Żelaźniewicz, 2002; Aleksandrowski and Mazur, 2002).

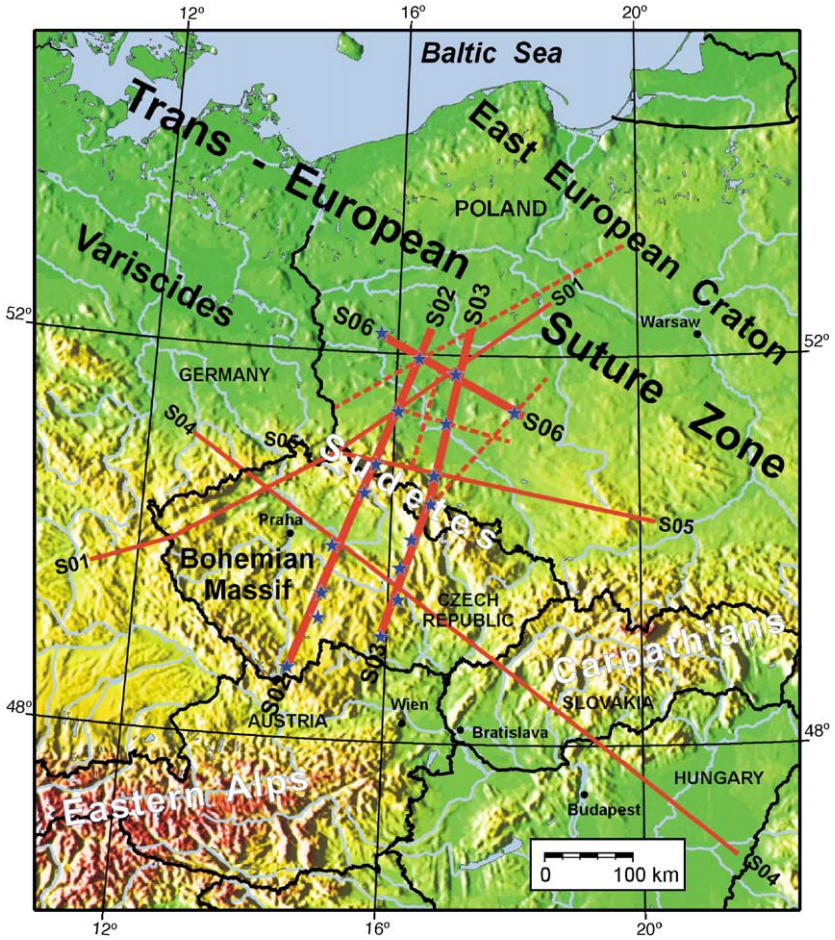

Fig. 1. SUDETES 2003 experiment map showing location of profiles (solid red lines for high-density profiles and dashed red lines for low-density ones), and shot points along profiles S02, S03 and S06 (blue stars) on the simplified background of the tectonic units around the Trans-European Suture Zone (TESZ) in Central Europe.

The SUDETES 2003 seismic refraction and wide-angle reflection experiment (Grad et al., 2003b) was carried out in June 2003 along six main profiles in SW Poland, SE Germany and Czech Republic, with the eastern extension to Slovakia and Hungary (Figs. 1 and 2). The experiment covered mainly the northern part of the Bohemian Massif and some of the neighboring Polish Basin (TESZ) to the northeast, and the West Carpathians to the southeast. In this paper we present detailed analysis of the crustal structure using three different techniques for two profiles across Sudetes Mountains: S02 and S03, and crossing them profile S06. From the geological point of view profile S06 runs along Wolsztyn High in the northern part of the study area and is crossed here almost perpendicularly by profiles S02 and S03. Further to the SW, profiles S02 and S03 run through the Fore-Sudetic Monocline, Fore-Sudetic Block, Sudetes Mountains and Bohemian Massif (Moldanubian). These terranes are separated by Odra Fault Zone, Marginal Sudetic Fault and Elbe Fault Zone, respectively.

2. Previous seismic investigations of the area

SUDETES 2003 experiment and surroundings, has been investigated by deep seismic sounding technique (e.g., Beránek and Dudek, 1972; Guterch et al., 1986, 1992; Aichroth et al., 1992; Mayerová et al., 1994; Grad et al., 2002a, 2003a; Hrubcová et al., 2005), surface waves (e.g., Neunhöfer et al., 1981; Wieland et al., 1987a,b; Novotný et al., 1995, 1997) and receiver function (e.g., Kind et al., 1995; Geissler et al., 2002; Wilde-Piórko et al., 2005). The crustal thickness of the Palaeozoic Platform in Poland, northeast of Sudetes, varies from 30–32 km beneath the Fore-Sudetic Monocline to 30–35 km beneath the Fore-Sudetic Block and Sudetes. In Czech Republic the crust of the Bohemian Massif is 30–40 km thick, thickening gradually from

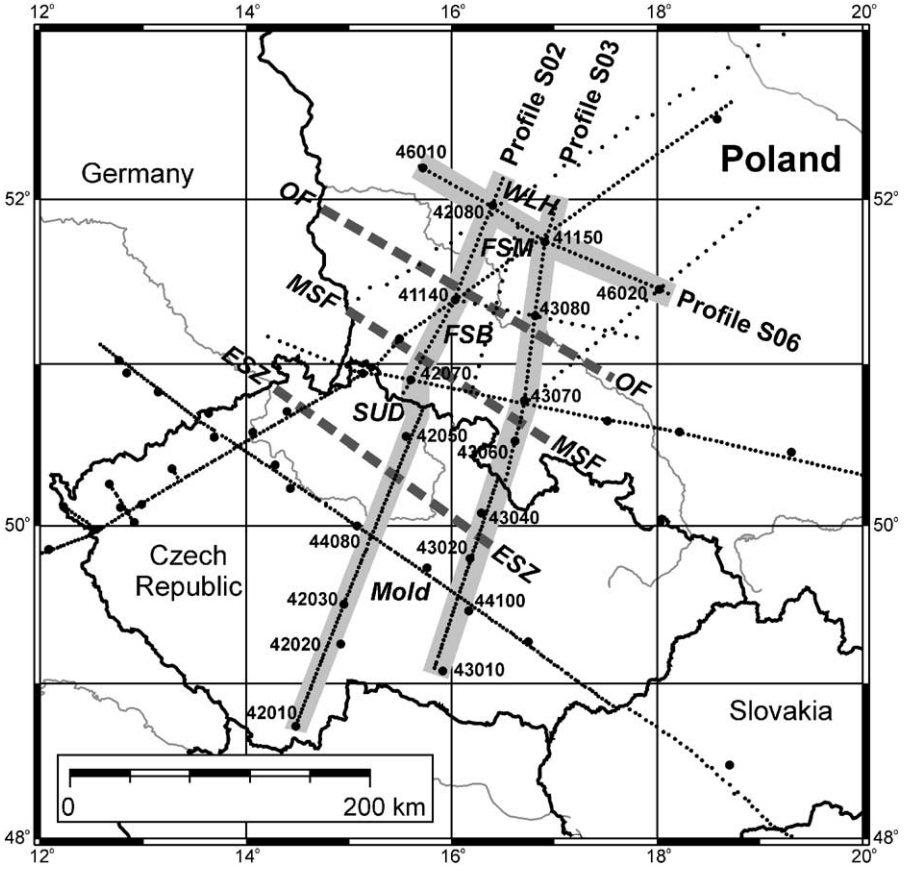

Fig. 2. Location of SUDETES 2003 seismic profiles with shot points (big dots) and receiver positions (points). Profiles S02, S03 and S06 are marked in gray and shot numbers are labeled. ESZ—Elbe Shear Zone; FSB—Fore-Sudetic Block; FSM—Fore-Sudetic Monocline; Mold—Moldanubian; MSF—Mid-Sudetic Fault; OF—Odra Fault; SUD—Sudetes Mountains; WLH—Wolsztyn High, Notice: all shots from SUDETES 2003 experiment were observed on each receiver positions along all profiles.

the northwest (Saxothuringian Zone) to southeast (Moldanubian Zone). The Moho depth has two maxima beneath the Sudetes (about 35 km) and in the southern part of the massif (about 40 km). The P-wave seismic velocities are relatively low (<6.0–6.4 km/s) down to depth of about 15 km, and the lower crust is character-

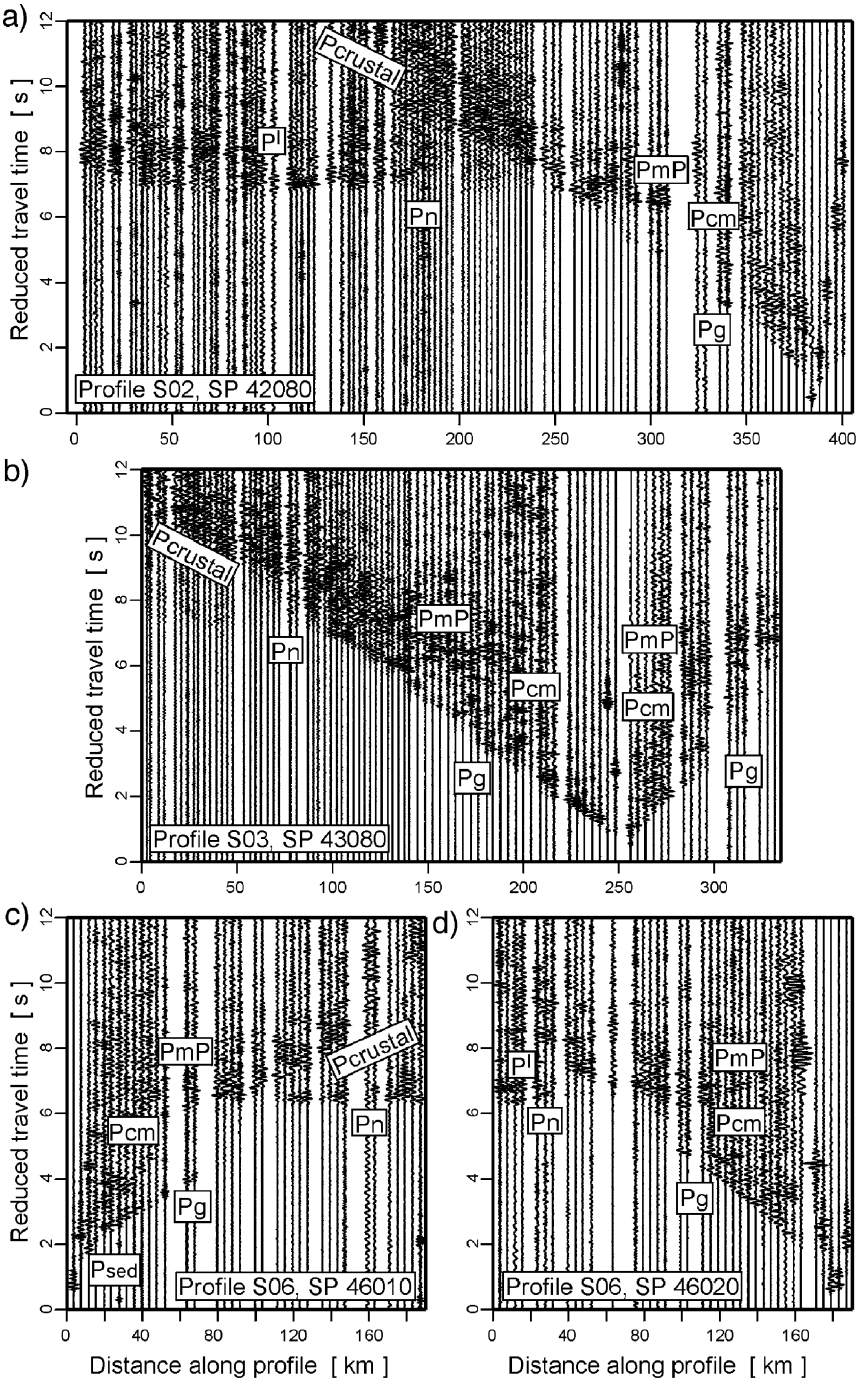

Fig. 3. Examples of trace-normalized, vertical-component seismic record sections for (a) SP 42080 on profile S02, (b) SP 43080 on profile S03, and (c) SP 46010 and (d) SP 46020 on profile S06. P_{sed}—waves refracted/reflected in sediments; P_g—waves refracted from the crystalline basement; $P_{crustal}$—extension of the P_g wave penetrated the lower crust and observed in the second arrivals; P_mP and P_n—reflected and refracted waves from the Moho; P^l—lower lithosphere phase. Reduction velocity 8.0 km/s, filter 2–15 Hz.

ized by P-wave velocity of 6.6–7.1 km/s. In the surroundings of the study area, crustal thickness reaches 40–50 km in the TESZ and EEC, and 23–30 km only in the Pannonian Basin and Carphathians (e.g., Grad et al., 2003a, in press; Kozlovskaya et al., 2004). To summarize, the crustal structure of the whole SUDETES 2003 area is not homogeneous, but in the area of S02, S03 and S06 profiles the crustal thickness is rather constant, amounting to 30–40 km.

3. Data acquisition and seismic wave field

The SUDETES 2003 experiment employed an up-to-date, 3-D implementation of the seismic refraction and wide angle reflection method (Fig. 1). The layout of the field part of the project consists of a network of recording profiles of a total length of 3450 km: six high-density profiles (S01–S06 with station spacing 3–4 km), and four low-density profiles (station spacing ~6 km). The recordings were done not only along profiles with in-line shots but also off-line ones (particularly in SW Poland) to obtain dense ray coverage (Figs. 1 and 2). Such data will allow 3-D modelling of the crustal structure, particularly for SW Poland and Sudetes Mountains. Altogether, 53 shots were fired with the charge ranging from 50 to 1000 kg (Grad et al., 2003b). Although there were considerable variations due to local conditions, the standard shooting configuration was to drill 5–10 boreholes to a depth of 30–40 m, and place 30–50 kg of explosives in each hole. The main seismic recording system employed was the single-channel RefTek 125 ("Texan") recorder. In addition to 920 "Texan" instruments, 61 other 3-component instruments were employed (for details see Grad et al., 2003b; Guterch et al., 2003b).

In this paper, data from SUDETES 2003 profiles S02, S03 and S06 have been interpreted. Profiles S02 and S03, crossing the Sudetes Mountains are almost parallel and are oriented nearly SW–NE. The third profile, S06, lies along the Wolsztyn High and crosses both previous profiles perpendicularly (Figs. 1 and 2). For purposes of this paper, only 2-D data were used (along all three profiles); nevertheless, the geometry allows to verify modeled structure beneath the crossing points of profiles. Profile S02 is 410 km long with 3 km spaced recorders. Nine shots were fired and recorded along this profile. All shots, except of two (SP 42020 and 44080), lie exactly on the profile. At the Poland–Czech Republic border this profile is not continuous, and its ca. 20 km shift (between shots 42050 and 42070) was done to pass round the town Jelenia Góra. However, in 2-D modelling the real distances were used and this perturbation can influence only very shallow structure, which is beyond of our method resolution. Profile S03 is 335 km long, with 8 shot points, and ca. 3 km

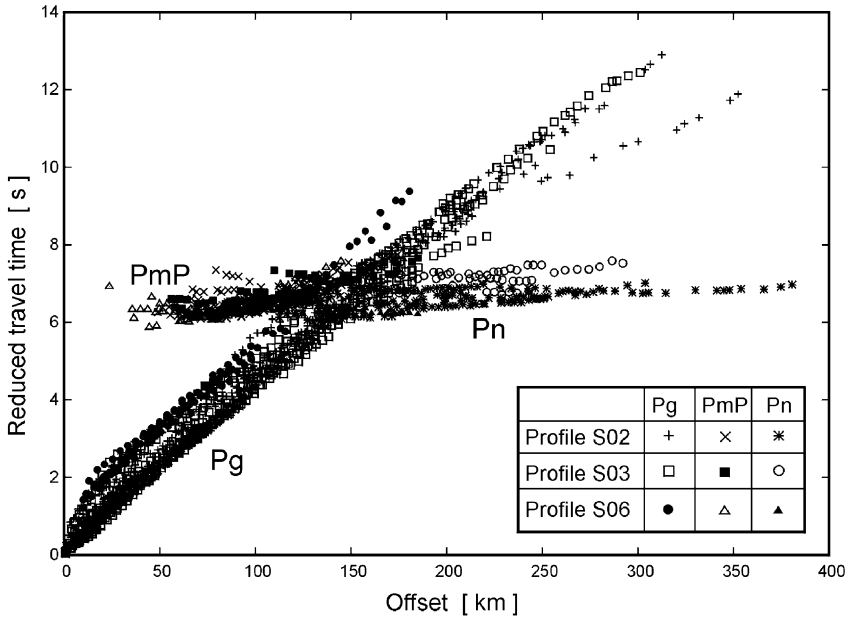

Fig. 4. Travel time picks for P_g, P_mP and P_n phases recorded at profiles S02, S03 and S06. Reduction velocity 8.0 km/s. Note 1–2 s scattering of travel times along most of the offset interval, which indicates variation of the crustal structure along profiles. Picks of P_g and P_n phases were used in the "smooth" tomography; all phases (with other phases) were included in JIVE3D inversion and ray tracing modelling.

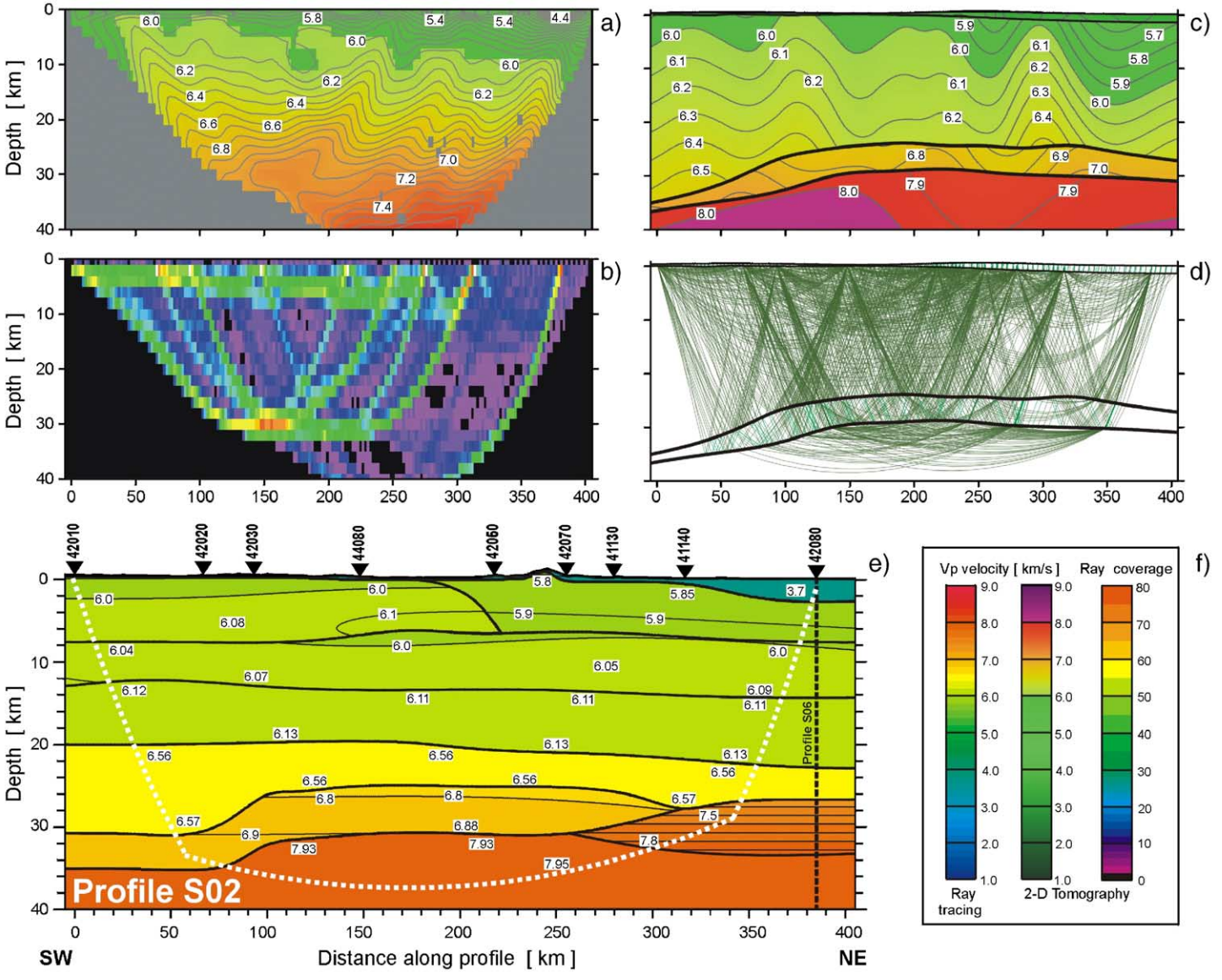

Fig. 5. Final models for profile S02; refracted wave travel time ("smooth") tomography (a) with ray coverage (b), joint reflected and refracted waves travel time tomography (c) with successful rays in last iteration (d), and ray tracing model (e). Scales in (f) show isovelocity colours and ray coverage. Numbers in squares are P wave velocities in km/s.

recorders spacing. The shortest profile, S06, is only 190 km long, with 4 shot points, and ca. 4 km recorders spacing.

In general, all profiles recorded good quality seismic data. Examples of seismic record sections from profiles S02, S03 and S06 are shown in Fig. 3. Main phases of refracted and reflected waves, namely P_{sed}, P_g, $P_{crustal}$, P_{cm}, P_mP, P_n and P^I, were used in derivation of crustal and uppermost mantle models. Although the area covered by profiles is large, the scattering of travel times for all phases is about 2 s only (Fig. 4). It could be mentioned here that the scattering of travel times for profiles from the TESZ area (for example, profile P4 and 3-D data from POLONAISE'97 experiment; profiles LT-2, LT-4, LT-5) reaches even 4–5 s (Grad et al., 2003a, 2005; Środa et al., 2002). In this paper we present detailed analysis of the crustal structure for profiles S02, S03 and S06 using three different techniques. Models obtained using different techniques are compared for all the above-mentioned profiles in Figs. 5–7, and examples of travel times calculated using ray tracing technique, synthetic seismograms and ray diagrams together with observed seismic sections are shown in Figs. 8–12. Summary of all crustal and uppermost mantle models is shown in Fig. 13.

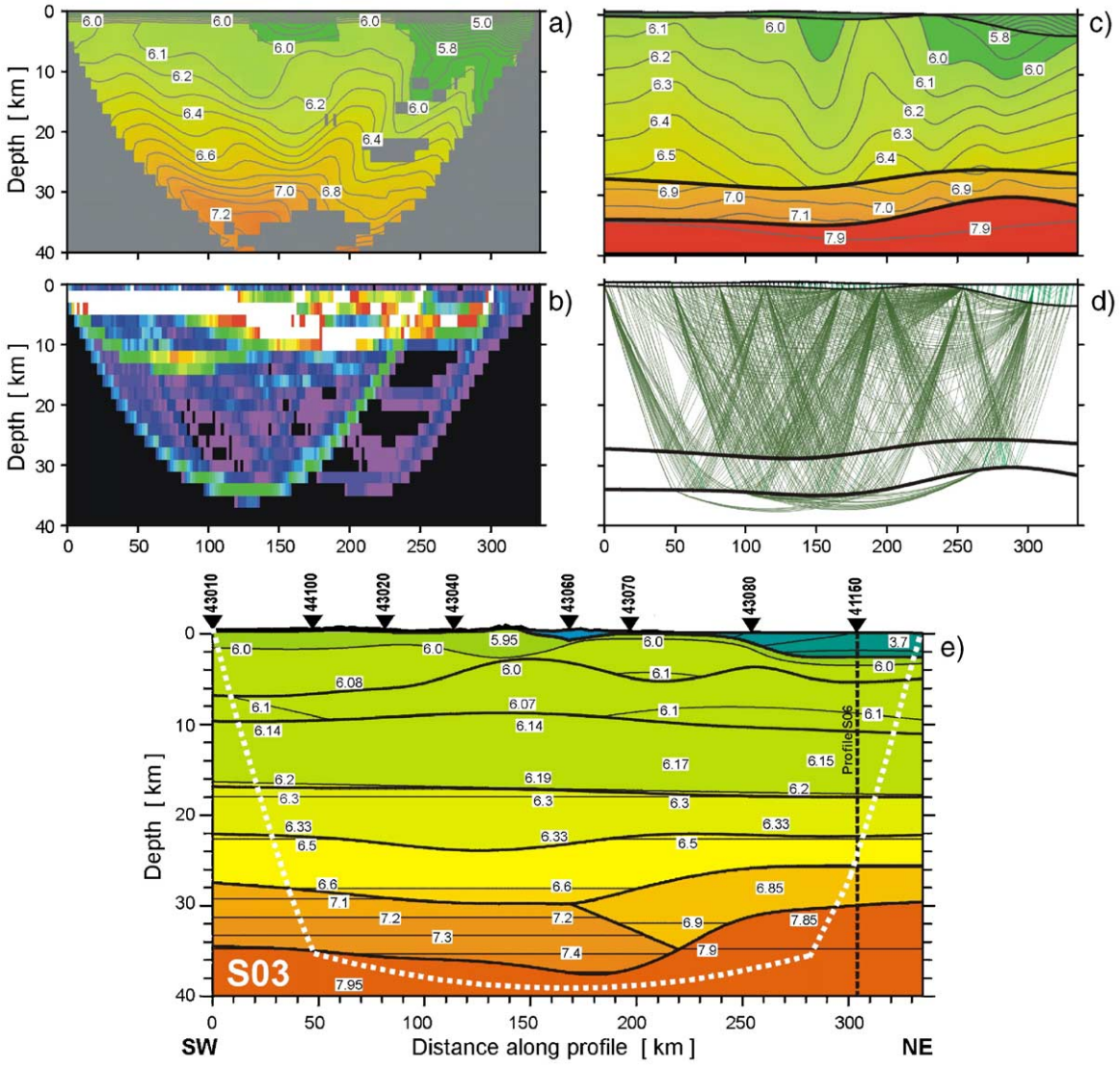

Fig. 6. Final models for profile S03; refracted wave travel time ("smooth") tomography (a) with ray coverage (b), joint reflected and refracted waves travel time tomography (c) with successful rays in last iteration (d), and ray tracing model (e). Numbers in squares are P wave velocities in km/s.

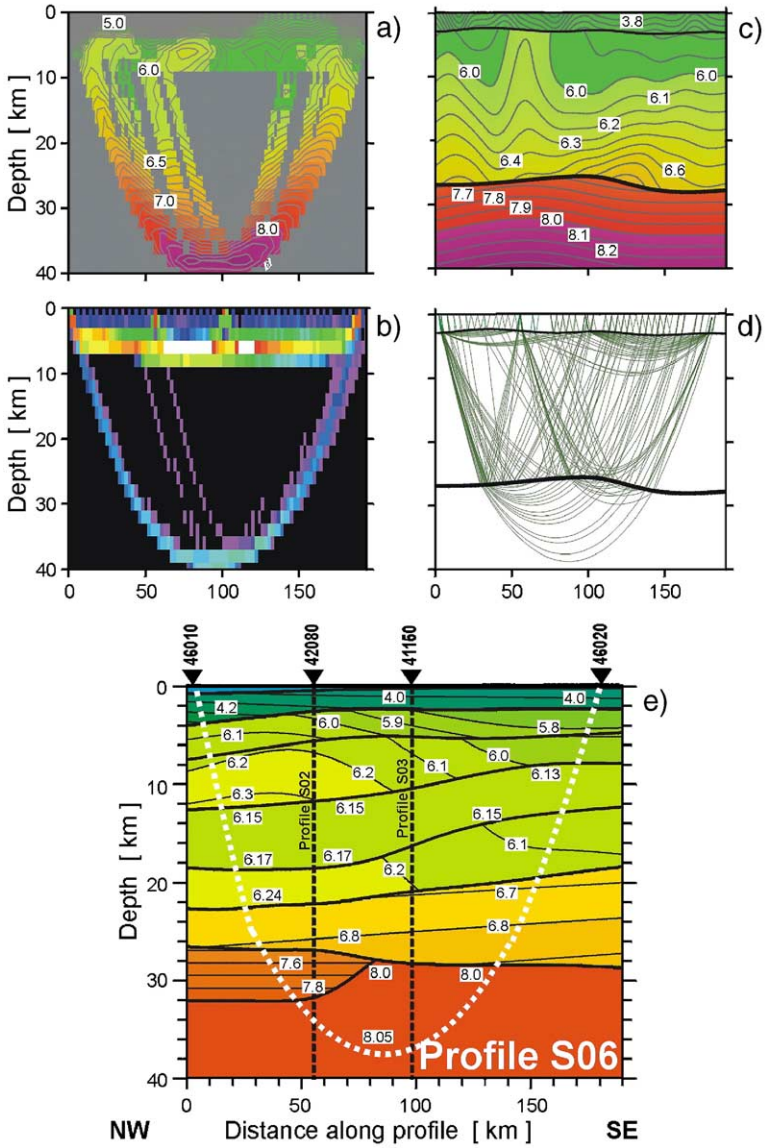

Fig. 7. Final models for profile S06; refracted wave travel time ("smooth") tomography (a) with ray coverage (b), joint reflected and refracted waves travel time tomography (c) with successful rays in last iteration (d), and ray tracing model (e). Numbers in squares are P wave velocities in km/s.

The seismic wave field recorded along profiles S02, S03 and S06 shows some regularities (Fig. 3), and are presented together with results of modelling (Figs. 8–12). In general, waves P_{sed} connected with the sedimentary cover are observed in the northern part of the study area, north of the Sudetes. The P_g waves from consolidated/crystalline basement are observed in the first arrivals up to ca. 140 km offset (Fig. 4). The travel times of P_g wave are almost straight lines, which indicates rather low velocity gradient in the upper crust. The continuation of P_g wave is very often well visible in the second arrivals as $P_{crustal}$ wave group, even up to 250–300 km offset (e.g., Figs. 3ab, 11 and 12ab). Strong reflected P_{cm} waves are connected with a boundary in the lower crust (zone of crust–mantle transition). Strong P_mP waves reflected from the Moho discontinuity are usually the strongest waves in the offset ca. 80–160 km. However, in some cases the P_{cm} wave is stronger, and the P_mP wave is not very well visible in the coda of P_{cm} group. Starting from the offset of 150 km, P_n waves refracted in the uppermost mantle occur as first arrivals. The apparent velocity of this wave is, in average, slightly lower than 8 km/s, as can be seen

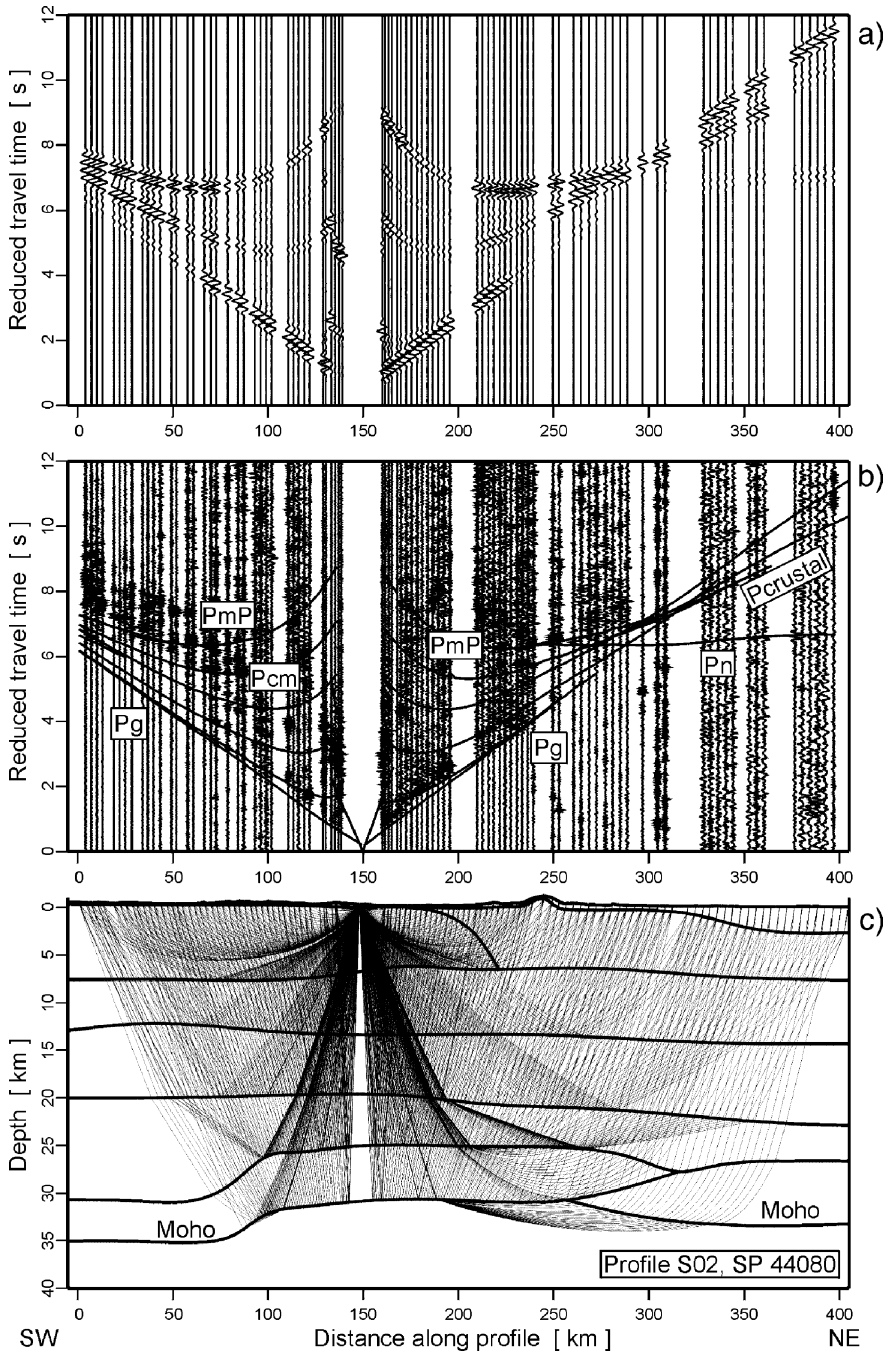

Fig. 8. Example of the ray-tracing modelling for profile S02, SP 44080; amplitude normalized synthetic seismograms (a), record section with theoretical travel times (b), diagram with refracted and reflected wave rays in the model. Reduction velocity 8 km/s, filter 2–15 Hz.

in Fig. 4. In a few record sections, waves P^{I} reflected from deep reflectors in the mantle lithosphere were found (e.g., Figs. 3a, 11a and 12a).

For profile S02, low velocity P_{sed} waves (apparent P-wave velocity <4 km/s) are observed only at the northeasternmost part for offsets up to 15 km. P_g waves in the Polish part of profile have velocities >5.8 km/s, and are strong up to 100 km offset. The extension of P_g waves ($P_{crustal}$) have an apparent velocity of 6.0–6.3 km/s, and are observed even up to 200 km offset. There is no evidence for high velocity lower crust (velocity >7 km/s) for the whole profile. For

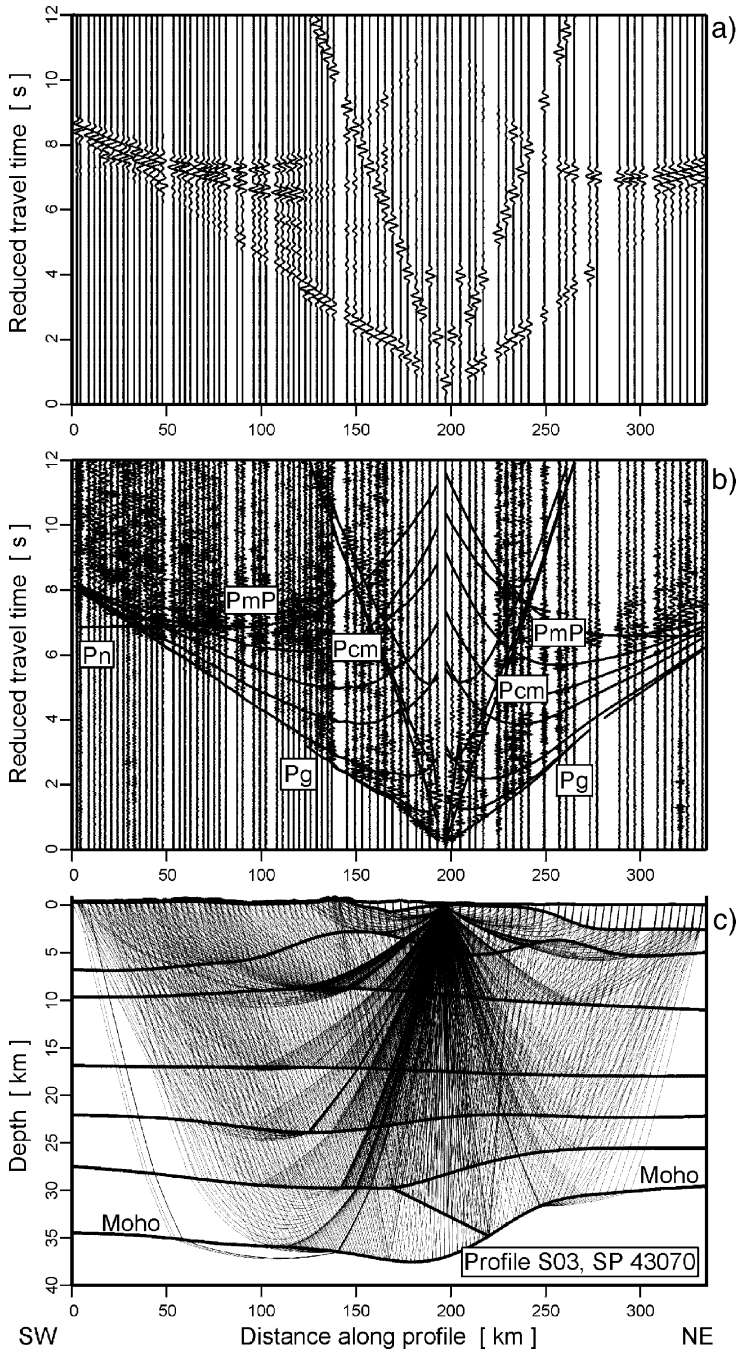

Fig. 9. Example of the ray-tracing modelling for profile S03, SP 43070; amplitude normalized synthetic seismograms (a), record section with theoretical travel times (b), diagram with refracted and reflected wave rays in the model. Reduction velocity 8 km/s, filter 2–15 Hz.

energy propagated in the crust in the northeastern direction the dumping zones at 250 km distance could be observed, which correspond to the Odra fault. The crust beneath profile is almost transparent, without strong mid-crustal reflectors. Strong reflections P_{cm} from the boundary near the Moho in the lower crust are observed for almost whole profile. In some cases, the P_{cm} wave is even stronger than P_mP (e.g., for shot points 42080 and 42020; Fig. 11a and b, respectively). Upper mantle refraction P_n is very weak in the SW part of profile and for SP 42010, 44080, 42050 it is almost invisible. Relatively strong P_n waves are observed for SP

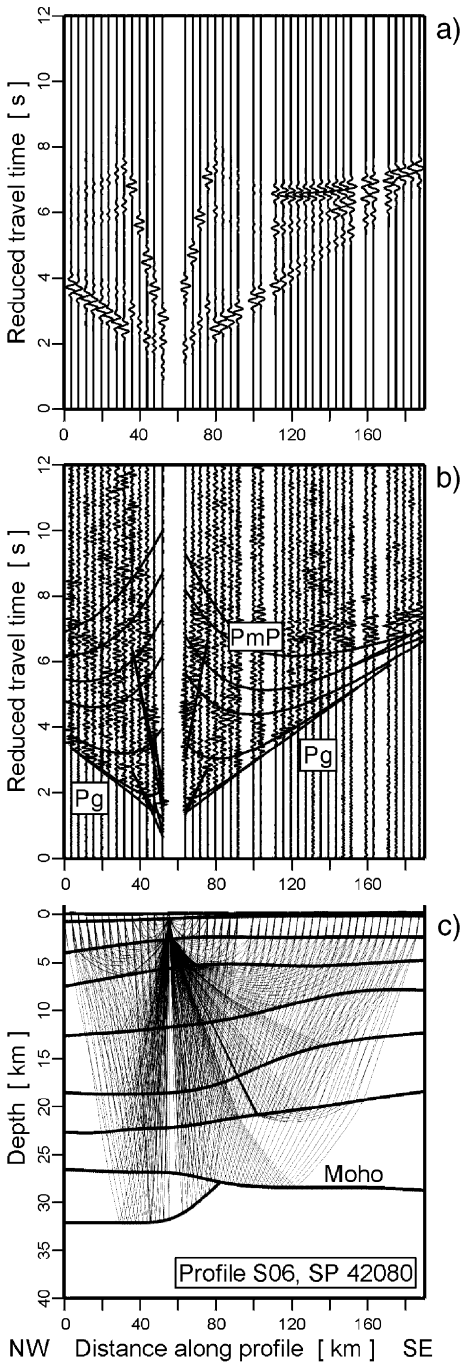

Fig. 10. Example of the ray-tracing modelling for profile S06, SP 42080; amplitude normalized synthetic seismograms (a), record section with theoretical travel times (b), diagram with refracted and reflected wave rays in the model. Reduction velocity 8 km/s, filter 2–15 Hz.

42070 and 42080 to the southwest (see for example Fig. 3a in the distance interval 100–200 km). For SP 41130, 41140 and 42080, very strong lower lithospheric reflections are observed, and for SP 42080 the P^{I} wave is very well visible up to the offset of 380 km (Figs. 3a and 11a).

For profile S03 the main characteristics of the wave field are very similar. The wave from sedimentary cover P_{sed} with relatively low velocity (about 4.5 km/s) exists only in the 30 km offset for SP 41150 in the northeastern part of profile. For the rest of profile P_g first arrivals with an apparent velocity of about 6 km/s are observed closely to all shot points. Strong P_g waves are observed up to 160 km offset (e.g., SP 43010 in Fig. 12b). Extension of P_g waves, $P_{crustal}$ waves, propagated with an apparent velocity of 6.0–6.5 km/s, are observed for SP 44100, 43080 and 41150 even up to 300 km offset. At 220–250 km along the profile, a damping zone could be observed, which blocks the energy propagation towards the northeast (the Odra fault zone, as in the case of profile S02). At the southwestern part of profile, in the crystalline crust, a few reflectors are observed. Beneath the Polish part of profile, the crystalline crust is almost transparent down to strong lower crustal reflector (P_{cm} wave). In the SW part of profile, this reflection is even stronger than P_mP reflection. P_n wave is observed only for SP 43080 and 41150. Additionally, strong lithospheric reflection P^{I} is visible at offset 250–300 km for SP 41150 (Fig. 12a in distance interval 0–60 km).

For the whole profile S06, slow first arrivals (V_p<4 km/s) are observed in 15 km offset, then P_g waves with velocities ca. 6 km/s are visible as strong first arrivals up to about 120 km offset. For shots 46010 and 46020, $P_{crustal}$ waves are visible for the whole 180 km length of the profile. The only one strong reflection is the P_mP reflection from the Moho, which is clearly visible in all four shots. Because the profile is short, P_n waves are visible only for edge shots, but are strong and clear (Fig. 3c, distance interval 120–190 km, and Fig. 3d, distance interval 0–40 km). For SP 46020, strong upper mantle reflection P^{I} is visible after P_n wave. This last observation together with data from profiles S02 and S03 proves the existence of the upper mantle reflector in the study area.

4. Derivation of the 2-D models of the structure

In the modelling of seismic data from SUDETES 2003 experiment for profiles S02, S03 and S06, three different methods were applied. First, “smooth” travel time tomography, was done using John Hole algorithms (Hole, 1992). These calculations were based on the first arrivals of P_g and P_n waves. Additionally, travel times of P_g waves were extended including second arrivals of

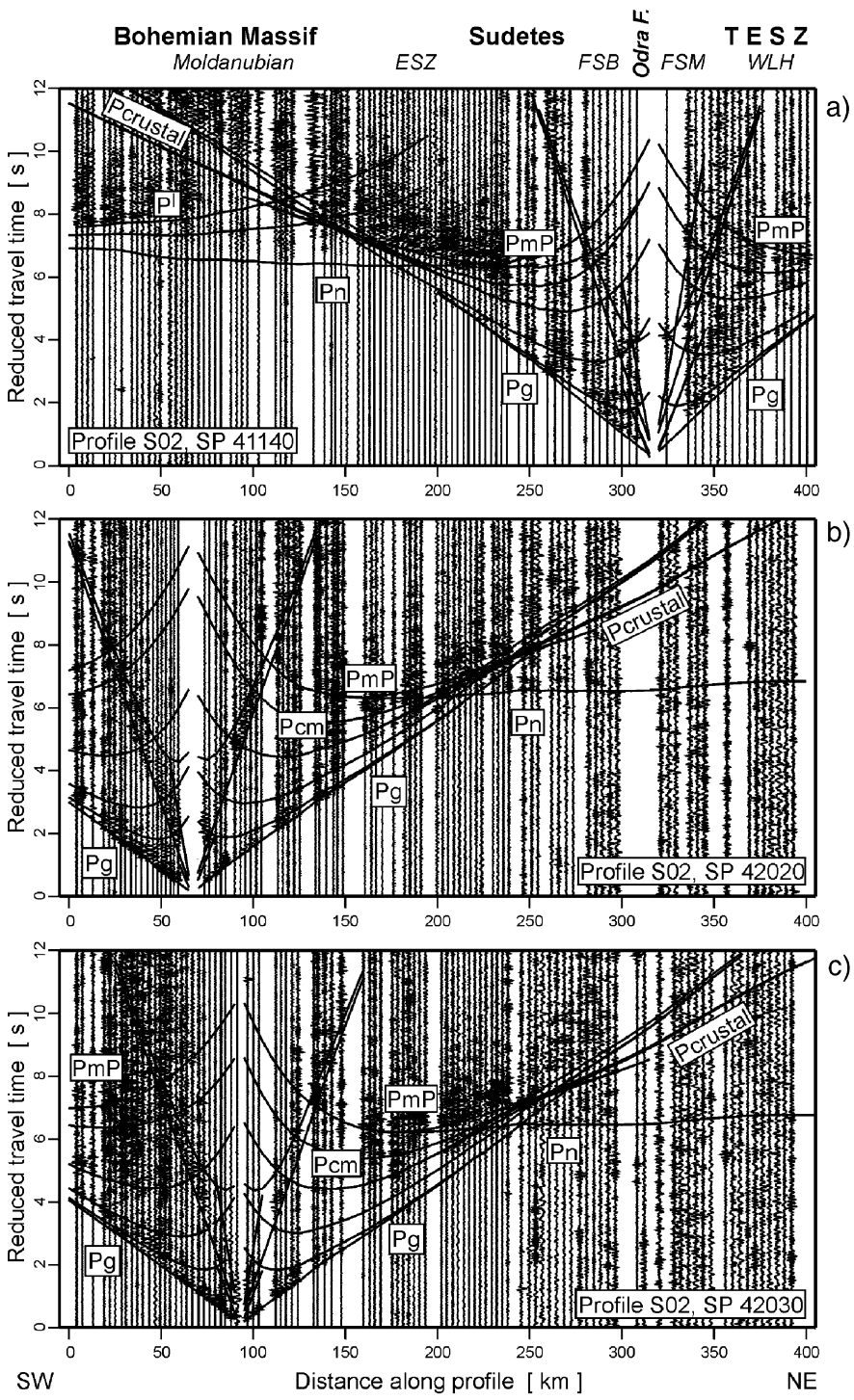

Fig. 11. Examples of the amplitude normalized seismic record sections for profile S02 with calculated travel times (lines) for shot points: SP 41140 (a), SP 42020 (b), and SP 42030 (c). Reduction velocity 8 km/s; filter 2–15 Hz; phase descriptions as in Fig. 3.

$P_{crustal}$ waves. Description of this kind of data selection and interpretation was presented by Majdański and Grad (2005). Next, the full 2-D ray tracing modelling was made with the use of all correlated refracted and reflected waves. SEIS83 package (Červený and Pšenčík, 1983) was used with program MODEL (Kommi-

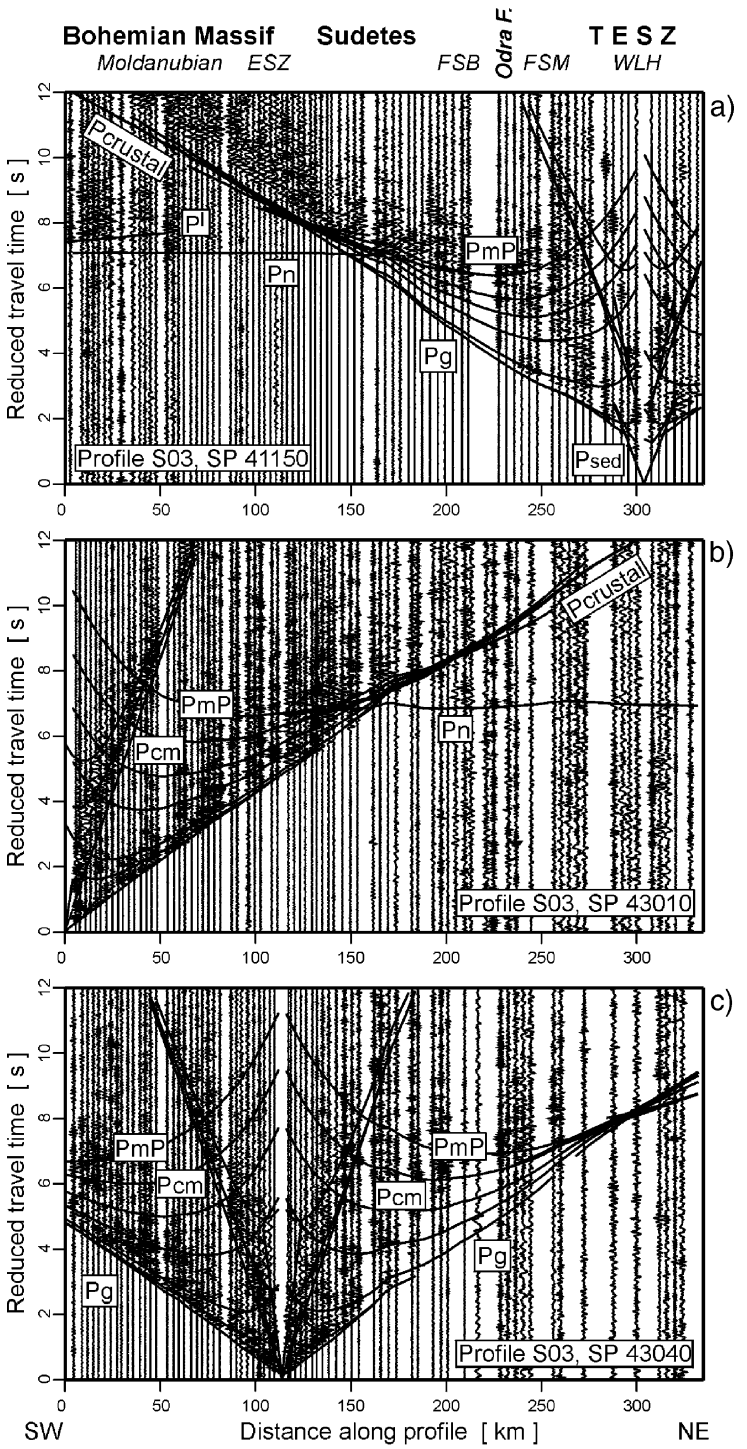

Fig. 12. Examples of the amplitude normalized seismic record sections for profile S03 with calculated travel times for shot points: SP 41150 (a), SP 43010 (b), and SP 423040 (c). Reduction velocity 8 km/s; filter 2–15 Hz; phase descriptions as in Fig. 3.

naho, 1998) and modified program ZPLOT (Zelt, 1994; Środa, 1999). At the end, a travel time tomography was performed with JIVE3D package (Hobro, 1999) for both refracted and reflected waves in four-layer models: sediments, crystalline upper and middle crust together, lower crust and the mantle.

4.1. "*Smooth*" tomographic inversion of refracted waves travel times

The fastest way to have the images of the structure is calculation of the first arrival tomography. Picking of the first arrivals is relatively fast and easy, and the algorithms are fast. Nevertheless, smooth model of the velocity distribution achieved in standard first arrivals travel time tomography is not sufficient to describe the structure. In particular, discontinuities with high velocities contrast (sediments–basement, lower crust–uppermost mantle) are imaged as a high velocity gradient zones. In such a case, the representation of "discontinuity" in the tomographic model is an isovelocity with a velocity being an average from velocities below and above the boundary. Another problem in the first arrival tomography is the lack of ray covering the lower crust. P_g waves cover usually the upper crust, and P_n waves—the uppermost mantle. So, the lower crust is not examined by rays where P_g and P_n waves only are used. To solve this problem, the use of $P_{crustal}$ waves (P_g wave extension) observed as second arrival was proposed (Majdański and Grad, 2005). The combination of $P_g+P_{crustal}$ waves allows to increase ray coverage in the lower crust and verify the velocities in this area. In the final inversion $P_g+P_{crustal}$ waves travel times together with P_n wave travel times give much more precise tomographic model.

In the "smooth" travel time tomography for the data from profiles S02, S03 and S06 the number of verified $P_g+P_{crustal}$ times (picks) used for this inversion is: 516 for S02 profile, 514 for S03 profile, and 151 for S06 profile (Fig. 4). The inversion starts from continuous 1-D model, which is an average for the data set.

This inversion is performed as a standard "smooth" travel time inversion for the crust only with the cell size of 2×2 km. In this step the input data are divided into three groups with a maximum offsets 20, 60 and 400 km, and next iterations include also previous data. This allows to fit as a first shallower part of the model (better covered) before deeper ones. For each iteration, parameters of smoothing are decreasing and there cover 12, 8 and 4 cells in horizontal, and 8, 4 and 2 cells in vertical directions. The whole process is repeated 4 times. After all 36 iterations we get a final model for the crust. In the next step, this model is used as a starting one for inversion of P_g and P_n waves travel times (Fig. 4), with extra P_n picks: 162 for S02 profile, 59 for S03 profile, and 101 for S03 profile. The P_g waves "freeze" the shallow part of the model (solution from the first step of iteration), while the P_n waves penetrate the uppermost mantle. This step of inversion is repeated 4 times the for whole data set with small smoothing (4 cells in horizontal, and 2 cells in vertical direction).

Results of "smooth" travel time inversion for all three profiles are presented in Figs. 5ab–7ab. Because this method can use only the refracted waves travel times, the best ray coverage is in the shallowest 10 km for all profiles. Although tomography cannot model a sharp velocity change (first order boundaries), the strong gradient areas can be interpreted here as boundaries. The biggest contrast of velocities is expected at the sediments–basement boundary. For velocities 4 km/s in the sediments floor, and 6 km/s in the topmost basement, this difference could reach 2 km/s, and the average isovelocity which best characterizes the boundary is 5 km/s. For the study area the lower crust is characterized by a velocity of 6.8–7.0 km/s, and the uppermost mantle has a velocity of 8.0–8.2 km/s (Grad et al., 2002b, 2003a; Hrubcová et al., 2005), so the Moho can be interpreted as the 7.3–7.5 km/s isoline. However, to investigate the shape of Moho it is suggested to use techniques different from the "smooth" tomography.

For profile S02 (Fig. 5a,b), isovelocities 5.8–6.0 km/s are observed near surface in the southwestern part of profile, indicating a lack of sediments in this area. In the distance about 200–250 km, lower velocities are observed ($V_p<5$ km/s), and are interpreted as sedimentary layer dipping toward the northeast. For profile S03 (Fig. 6a,b), at 0–120 km and 200–230 distance along profile no low velocities characteristic of sediments are observed. For the rest of profile, velocities corresponding to sediments are visible with isolines dipping toward the northeast as for profile S02. For 210 km distance, high velocities near surface were found. Isolines in the middle and lower crust suggest almost horizontal structure with no strong contrasts. For profile S06 (Fig. 7a,b) the situation differs, because practically for the whole length of profile low velocities ($V_p<5$ km/s) and high velocity gradient are observed in the uppermost part of profile. This may be interpreted as 2–3 km thick low velocity sediments. Just beneath the sediments, velocities typical for the crystalline crust ($V_p>6$ km/s) are visible. In all three profiles isovelocities characteristic for Moho ($V_p=7.3$–7.5 km/s) were found at depths 32–36 km over the whole area, showing rather flat structure in the lower crust and uppermost mantle.

4.2. Forward modelling by ray tracing with SEIS83

The next approach used in interpretation was the ray tracing technique, where apart of all travel times of

refracted waves, also all identified and correlated reflected waves were additionally used. They provide the basis for the modelling of the velocity distribution and depths of seismic boundaries in the crustal and uppermost mantle models. During modelling we applied ray tracing calculations of travel times and synthetic seismograms for which we used interactive version of SEIS83 package (Červený and Pšenčík, 1983) with program MODEL (Komminaho, 1998) and modified program ZPLOT (Zelt, 1994; Środa, 1999). Basically P waves data were used for modelling, but some short offset S wave data (in the vicinity of shot points) were also used to assure correct amplitude of synthetic seismographs.

For profile S02 (Fig. 5e) the ray tracing model shows a small differentiation of the upper crust structure. The low velocity (V_p<4 km/s) sediments are almost absent in the southwestern part of profile (Bohemian Massif), while towards northeast their thickness increases reaching 3 km in the end of profile (see also Grad, 1991; Grad et al., 1991). Velocities in the upper crust are changing along profile from 6.0–6.1 to 5.9 km/s, and the change is placed at about 210 km of profile (ca. 30 km SW of Sudetes Mountains main ridge). The upper crust is characterized by small velocity gradient, and the first strong reflecting boundary was found at 20 km in the SW, and 23 km in the NE part of profile. Velocity contrast for this boundary is ca. 0.4 km/s and this boundary is documented almost along the whole length of profile. Next reflection is from a boundary just above the Moho. In the northeastern part of profile, the reflection from it (P_{cm}) is even stronger than the Moho reflection (Fig. 3a). The lowermost crust velocity is 6.9 km/s. In the northwestern part of profile the lowermost crustal velocity cannot be determined because we do not observe refracted waves from this layer. The velocities ca. 7.5 km/s were assumed there to explain very strong reflection, which fit well synthetic seismograms. The Moho boundary lays at 31 km depth in the central part of profile, dipping to 35 km toward SW and to 33 km toward NE directions. Velocities beneath Moho are low, ca. 7.95 km/s. In the upper mantle two reflectors were discovered at depths of 55–58 and 62–70 km and are well documented in the distance 100–250 km (Fig. 13a).

For profile S03 (Fig. 6e) low velocity sediments (V_p<4 km/s) are observed only in NE end of profile (2–3 km thickness). The consolidated crust (V_p~6 km/s) is almost horizontal. Velocities are changing from 5.95 km/s near the surface to 6.3 km/s at 20 km depth, and to 6.6 km/s at 30 km depth. Boundaries in the middle crust have got small velocity contrasts, 0.05–0.1 km/s. The lowermost crust in SW part of profile (0–170 km) is characterized by high velocity, ~7.2 km/s, and velocity contrast >0.5 km/s at depth ca. 29 km. In the NE part velocities are 6.8–6.9 km/s, and the velocity contrast is not so large (~0.3 km/s). The Moho boundary occurs at 35–37 km depth beneath the SW and central parts of profile, and rises to 30 km depth in the NE part. The upper mantle velocities are rather low, about 7.9 km/s (compare apparent velocities of reciprocal travel times of P_n waves from SP 41150 and 43010 in Fig. 12a,b). One lower lithospheric reflector was found at a depth of 53–56 km (Fig. 13b), but it is documented only from recordings in SW direction (no reciprocal travel times).

For profile S06 (Fig. 7e) the ray tracing model shows 2 km thick sediments, which are dipping to ca. 4 km depth in the NW end of profile. Three boundaries in the middle crust are dipping a few km toward NW. The velocities in these layers are 6.0–6.25 km/s in the NW part, and are by 0.2 km/s higher than in the SE part of profile. The velocity contrast at reflectors in this complex are rather small, ~0.05 km/s only. The boundary between middle and lower crust is much stronger (~0.5 km/s contrast); reflector at 23 km is rising to 18 km at SE end of profile. The lower crust velocity is ca. 6.8 km/s. The Moho boundary is placed at 32 km depth in the NW part, and at 29 km in the middle and SE parts of profile. However, the shape of the Moho and velocity distribution of the lower crust in the NW part is not well resolved, because strong reflection from 27 km depth boundary blurs all information from below. So this part of the model was prepared to be consistent with the good quality data from the crossing profile S02. In the upper mantle a reflector at 43 km depth was found (Fig. 13c).

4.3. Joint inversion of velocity and boundary depth with JIVE3D

After preparing the ray tracing models, join reflection and refraction tomography was performed for SUDETES 2003 data with the use of program JIVE3D (Hobro, 1999). This package allows to fit simultaneously the velocity distribution and the shape of boundaries for 3-D; however, for profiles S02, S03 and S06 we used only 2-D approach. Using ray tracing model it was possible to identify all important seismic phases (the strongest reflections) and gather both reflected and refracted waves travel times. For profiles S02 and S03 the initial four-layer models were constrained, which contain (1) sediments, (2) upper and middle crust, (3) lower crust and (4) upper mantle. The

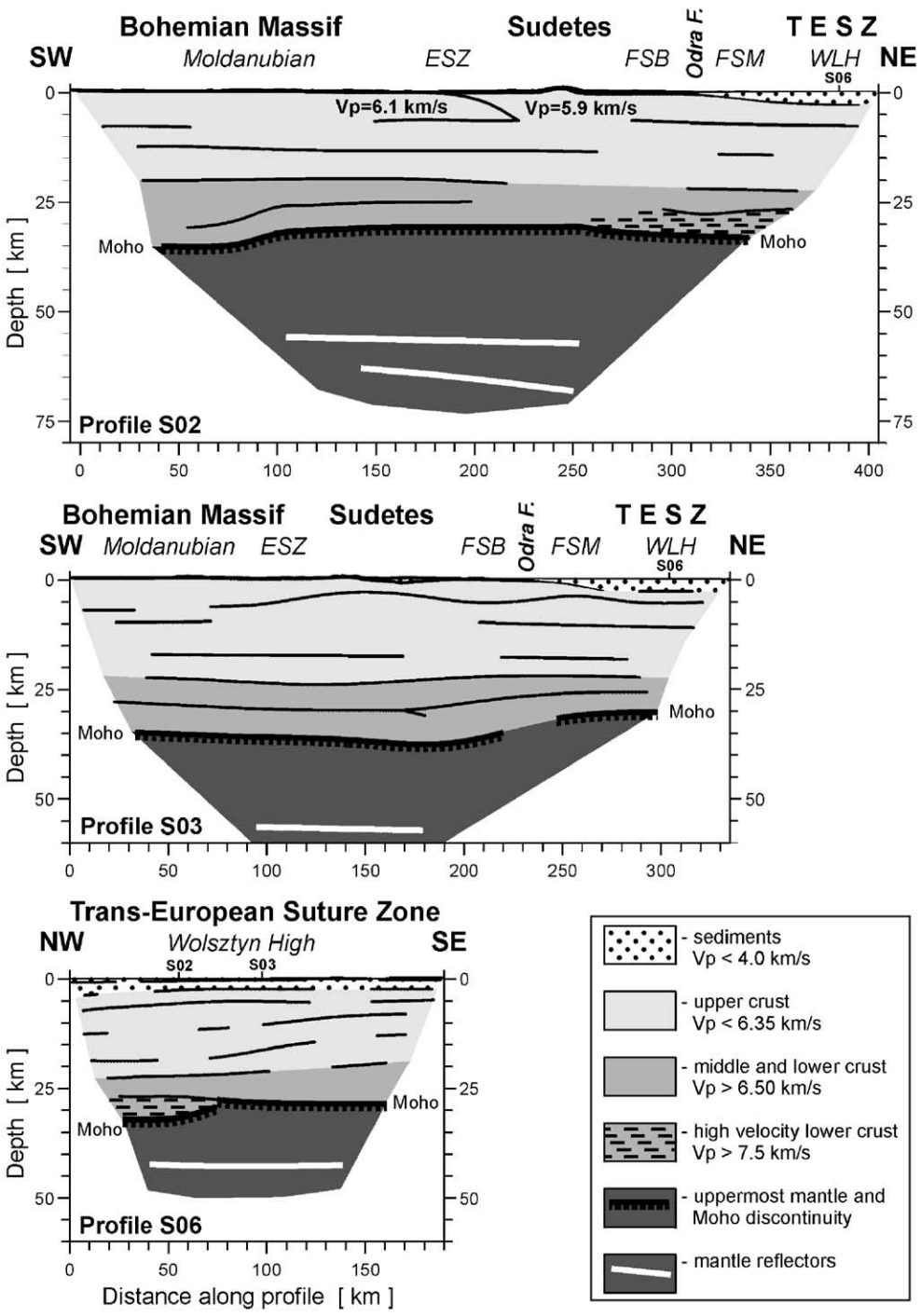

Fig. 13. Generalized two dimensional models for the crust and upper mantle for profile S02 (a), S03 (b) and S06 (c). Only the areas covered by rays are shown; solid lines show elements of reflectors (seismic boundaries) verified by reflected waves. White, solid lines—location of possible mantel reflections. ESZ—Elbe Shear Zone; FSB—Fore-Sudetic Block; FSM—Fore-Sudetic Monocline; TESZ—Trans-European Suture Zone; WLH—Wolsztyn High.

corresponding groups of waves for each layer are: (1) P_{sed}, (2) P_g, $P_{crustal}$ and P_{cm}, (3) P_mP with refraction in the lower crust, and (4) P_n waves travel times (picks). For profile S06 due to lack of P_{cm} wave, initial three-layer model (sediments, crust, upper mantle) was constrained. The whole data set is larger than that used for "smooth"

tomography (Fig. 4), and contains 1111 picks for profile S02, 868 for profile S03, and 252 for profile S06.

Starting models for all profiles were prepared with horizontal layers and with vertical velocity gradient. The inversion path was the simplest one, included all phases from the beginning, and the inversion of velocities in layers and shape of reflectors was done simultaneously. The results were obtained after 60 iterations (in 6 loops) with decreasing smoothing strength (chosen and changing in each loop after 10 iterations). The regularization strength is measured on a logarithmic scale, so it is drastically reduced during inversion (Table 1). The regularization strength parameters have been chosen with trial and error method to keep the maximum value of hit rate (successful rays). Increasing number of steps with a smaller reduction of smoothing would slightly increase the hit rate, and would much increase the calculation time. As shown in Table 1, the regularization path is different for each profile. The greater number of missing hits is connected with P_n phase (>50% of all P_n picks), but the crustal phases are calculated successfully. A similar difficulty with P_n phase modelling is met very often using ray theory approach for a small velocity gradient medium (as the uppermost mantle usually is) and a complex shape of boundary (Moho in the case). The final model hit ratio was 75% of all used data and in some stages of modelling it was even over 80%. In the last model, after the boundary shape changes, the P_n picks were the most missing ones. Nevertheless, the crust itself is well covered by rays, and velocities are well documented. The values of chi squared (χ^2 characterizes the fit to data) decrease significantly during the inversion process, and show that the final models are well-fit to the data set. This modelling was performed to make "automatically" a completely independent model, to confirm (or confront) results of ray tracing modelling. Additionally, it was a test for this kind of technique before applying it to full 3-D modelling, where this method can show, hopefully, its full power. The final models are shown in Figs. 5cd–7cd together with the coverage by rays of refracted and reflected waves. In general, they agree well with the results of ray tracing modelling.

Table 1
Parameters in inversion for program JIVE3D

Iteration	Profile S02			Profile S03			Profile S06		
	Hit rate	Reg.	χ^2	Hit rate	Reg.	χ^2	Hit rate	Reg.	χ^2
1 1	72%	–	24.78	80%	–	43.49	69%	–	72.44
1 10	67%	0.0	26.38	80%	0.0	43.40	64%	−1.0	43.27
2 10	66%	−1.0	25.36	80%	−1.0	43.31	68%	−2.0	52.84
3 10	68%	−2.0	23.41	75%	−2.0	37.36	67%	−2.5	35.79
4 10	66%	−3.0	14.63	76%	−3.0	26.76	65%	−3.0	25.96
5 10	68%	−3.5	11.15	70%	−4.0	14.50	64%	−3.5	25.16
6 10	73%	−4.0	9.12	73%	−5.0	8.53	66%	−4.0	13.19

Iteration—loop number (from 1 to 6) and iteration in loop (1 or 10); Hit rate—percent of successful rays; Reg.—regularization strength parameter for the velocity field smoothing; χ^2 —average value for all shots and all phases in iteration.

In the model for profile S02 (Fig. 5c,d), we observe that main elements of the structure (shape of boundaries, velocities in particular layers) agree well with ray tracing model. The shape of the Moho boundary differs in the edges of both models, but these parts are not covered by rays, and the observed effect is artificial. The northeastern part of the lower crust differs from ray tracing model, but as it was mentioned before, in wave field there is no information about waves refracted in this layer, so there is no information about velocity in this layer. In the ray tracing model the velocity in the lower crust was assumed to fit in the best way synthetic and observed amplitudes of reflected waves. So, this value was determined indirectly, not in the sense of travel times. Results from profile S03 (Fig. 6c,d) show that shape and depth of boundaries agree almost perfectly with those in ray tracing model (Fig. 6e). The sedimentary layer in the northeastern end of profile is 2–3 km thick. Also, small differentiation of the basement velocity is similar to those in the ray tracing model (lower in the northeastern part and higher in the southwestern part). In general, the upper and middle part is characterized by a small gradient of velocity and velocities from 5.8–6.1 km/s at the basement top, to 6.4–6.5 km/s at a depth of 26–28 km. Also, a similar contrast of velocities was obtained between the middle and lower crust (~0.5 km/s), and particularly high velocities, of 6.9–7.1 km/s, were found in the lower crust. Model for profile S06 is simple because the data set is small (only 4 shot points for this profile). Therefore, a simple three-layer structure was assumed, with two first order boundaries (sedimentary cover–crystalline crust and crust–upper mantle). The assumption of "smooth" crust (with no separate lower crust layer) produces some disagreement. Instead of high velocity lower crust (layer with velocity 6.8 km/s), a smooth change of velocity in the lower crust is observed. The shape of boundaries agrees, but in the northwestern part the model the strongly reflecting boundary does not correspond to the Moho boundary. It is the same situation as in on the very same area for profile S02. Because of the lack of data on this part of profile, there is no information on the Moho, and cannot be modeled here.

4.4. Mantle lithosphere reflectors

In some record sections, it is possible to see very strong P^I waves in the second arrivals, 1 s after P_n phase. This phase, observed for shot points located in the northern part of discussed area, is much stronger than P_n and has an apparent velocity 8.5 km/s. For profile S02 it is possible to see even two lower lithospheric reflections of this kind, but the second one is not so strong. However, there is no data to confirm these reflections for waves propagated northward from the shot points in the southern part of investigated area. Because of that, it was not possible to localize these reflectors precisely. The velocity differences at these boundaries were fitted to produce a correct synthetic amplitude and were proposed as a small positive contrast of velocity, 0.2 km/s. Our suggestion for these mantle reflectors is shown at the ray tracing models (Fig. 13). This stronger mantle reflector is placed at 60–66 km depth, and is deepening northward. Similar reflected wave P^I is observed along profile S03, but for one shot point only. We suggest that this is the same mantle reflector as in profile S02, with the same 0.2 km/s velocity contrast, but shallower, at a depth of 55–58 km. Profile S06 is too short to observe clearly this deep reflector, although later than P_n phase is observed. The corresponding reflector is located at 42 km depth and seems to be flat.

Summarizing, the mantle reflectors stretch beneath the Sudetes Mountains, deepening toward the northwest (Fig. 13). Additionally, a shallower reflector beneath profile S06 seems to be a separate one. As mentioned before, we are not able to verify the details of these reflectors using only this data. We believe that, after including other data from SUDETES 2003 experiment, this problem will be resolved.

5. Discussion of results and conclusions

The SUDETES 2003 experiment is the fourth from a series of large seismic refraction and wide-angle reflection experiments performed in 1997–2003 in Central Europe, and it covers the gap between areas of POLONAISE'97, CELEBRATION 2000 and ALP 2002 experiments. The experiment covered mainly the northern part of the Bohemian Massif and some of the neighboring Polish Basin (TESZ) to the northeast, and the West Carpathians to the southeast. In this paper we present models of the crustal structure beneath three profiles (S02, S03 and S06) crossing the Sudetes Mountains from the Bohemian Massif (Moldanubian), to Fore-Sudetic Block, Fore-Sudetic Monocline and Wolsztyn High.

The seismic data are in general of good quality, and in 2-D modelling along profiles S02, S03 and S06 three different methods were applied. The first, "smooth" travel time tomography (Hole, 1992), was based on the first arrivals of P_g (extended to include second arrivals of $P_{crustal}$ waves) and P_n waves. The second, the full 2-D ray tracing modelling was done using all correlated refracted and reflected waves (SEIS83 package; Červený and Pšenčík, 1983). The third method was travel time tomography for both refracted and reflected waves in multi-layer models using JIVE3D package (Hobro, 1999).

In spite of different interpretation techniques used, the models of the crustal structure show common characteristic features (Fig. 13). The low velocity ($V_p <$ 4 km/s) sedimentary layer was documented in the northeastern part of the study area. Its thickness increases towards the northeast, reaching 2–3 km in TESZ (Wolsztyn High). In the Sudetes and Bohemian Massif, sediments are almost absent. The topmost basement has in general a velocity of 5.8–6.0 km/s. Beneath profile S02, the basement of the Bohemian Massif has slightly higher velocities (6.0–6.1 km/s) than those south of the Sudetes (5.8–5.9 km/s). The site of this change correlates with the Sudetes (at about 210 km of profile, ca. 30 km SW of the Sudetes Mountains main ridge). The upper crust is characterized by small velocity gradient, and velocities at ca. 20 km depth are 6.15–6.25 km/s. A few reflectors were found in the upper crust with rather small velocity contrast of 0.05–0.1 km/s. The strongly reflecting boundaries were found at 20–23 and 25–28 km depth with a big velocity contrast (about 0.4 km/s). The highest velocities in the lowermost crust are 6.8–7.2 km/s. In the northeastern part of profile S02, in the lower crust, velocities of ca. 7.5 km/s were assumed to explain the observed very strong reflections. In general, the crust of the Bohemian Massif is slightly thicker (33–35 km) than in the northern part of the area. Velocities beneath Moho are relatively low, being 7.95 km/s.

Comparing crustal models in the crossing points of profiles, some disagreement in velocity could be detected. Beneath the crossing point of profiles S02 and S06 (in SP 42080; compare Figs. 5e and 6e), velocities in each layer of the crust are by about 0.1–0.2 km/s bigger for NW–SE direction (profile S06) than for SW–NE direction (profile S02). For the second crossing point (SP 41150, profiles S03 and S06) such an effect is not observed. The disagreement of veloci-

ties in the crossing point of 2-D profiles could not be interpreted automatically as an anisotropy. However, in the neighboring area of Bohemian Massif the 1.5–2.5% anisotropy was found from the azimuthal velocity variations of P_g waves (Růžek et al., 2003; Vavryčuk et al., 2004).

On the basis of well recorded reflected waves from the lower lithosphere (P^I), mantle reflectors were discovered at depth interval 40–70 km. Beneath profile S06, reflector at a depth of about 42 km. Similar reflectors occurring 10–15 km deeper than Moho, were found previously beneath POLONAISE'97 profiles in the TESZ area (Grad et al., 2002a). Such a reflector, following the Moho shape, but 10–15 km deeper, seems to be a common feature for the wide area of TESZ. In the upper mantle of the Sudetes and Bohemian Massif, this kind of lithospheric reflector was not discovered. Instead, beneath southwestern and central parts of profiles S02 and S03, two reflectors were discovered much deeper, at 55–58 and 62–70 km. It should be underlined, that exactly in the same depth range (55–58 km), mantle reflector was found in the Bohemian Massif beneath profile CEL09 (Hrubcová et al., 2005).

Apart of new results for the geology and tectonics of the area, some conclusion could be drawn about different techniques used. The initial point for all techniques of interpretation is the identification and correlation of regular refracted and reflected waves. This seems to be easy, particularly for 2-D data along profiles. However, in the data from SUDETES 2003 experiment some problems arise related to mid-crustal reflections. In the upper and middle crust they are usually weak, and do not correlate between profiles. This can also mean, that they are local, and are not characteristic for the whole area. On the other hand, the strongest reflected waves P_{cm} from horizons in the lower crust mask reflection from the Moho. In the identification of P_mP wave corresponding P_n wave could help, but in many cases it is also very weak. These problems could be even larger in the 3-D case.

The "smooth" tomography using first arrivals is the fastest way to have the first images of the seismic structure model. Such a model, however, does not describe the structure sufficiently well, particularly discontinuities with high contrast of velocities, which are imaged as high velocity contrast zones. Another problem is the lack of rays covering the whole crust, particularly the lower crust. The use of $P_g+P_{crustal}$ waves could help to solve it. The "smooth" tomography seems to be more effective for strongly differentiated areas, with large changes in depth of the main boundaries (e.g., for long-range profiles P4 and CEL05; Grad et al., 2003a, in press).

The "classical" ray tracing is still one of the techniques giving the best models of the structure, but the trial-and-error process is extremely time consuming. The advantage of this method is using, apart of travel times of refracted and reflected waves (both P and S), synthetic seismograms to control velocity gradients in layers and velocity contrasts at seismic boundaries. A "manual" control of the modelling helps avoid artificial effects, which are sometimes produced in the tomographic inversion process.

Intermediary for the two above mentioned techniques is travel time tomography for both refracted and reflected waves in multi-layer models. In this method the model is determined practically in the stage of correlation (in the sense the number of layers and corresponding travel times). In the process of inversion, the best fit model is calculated only. As can be seen from not very complex SUDETES 2003 data, the first hit rate is rather high (70–80% in Table 1), although χ^2 has a big value. Next iterations give significant improvement of χ^2, and the hit rate about 70%. The most numerous missing rays are P_n phases, absent after the boundary shape changes. The method is quite fast, and final models in general agree well with results of ray tracing modelling.

To summarize, in the 2-D case the "classical" ray tracing method gives the best model of the structure. However, because it is very time consuming, its application in the 3-D case seems to be unrealistic. The ray tracing method could be helpful in the process of identification and waves correlation, as well as determination of number of layers, but not in 3-D trial-and-error modelling of tens, or even hundreds of record sections. The "smooth" first arrival travel times tomography, although very fast, is not satisfactory to describe the complex structure either. So, the best candidate in 3-D case seems to be travel time tomography for both refracted and reflected waves in multi-layer models. The inversion process should be under very careful control, including amplitudes verification by synthetic seismograms. The travel time tomography for both refracted and reflected waves in multi-layer model applied in 3-D modelling will show, hopefully, its full power.

References

Aichroth, B., Prodehl, C., Thybo, H., 1992. Crustal structure along central segment of the EGT from seismic–refraction studies. Tectonophysics 207, 43–64.

Aleksandrowski, P., Mazur, S., 2002. Collage tectonics in the northeasternmost part of Variscan Belt: the Sudetes, Bohemian Massif. Geol. Soc. London Spec. Publ. 201, 237–277.

Beránek, B., Dudek, A., 1972. The results of deep seismic sounding in Czechoslovakia. Z. Geophys. 38, 415–427.

Brueckl, E., Bodoky, T., Hegedűs, E., Hrubcová, P., Gosar, A., Grad, M., Guterch, A., Hajnal, Z., Keller, G.R., Špičák, A., Sumanovač, F., Thybo, H., ALP 2002 Working Group, 2003. ALP 2002 seismic experiment Stud. Geophys. Geol. 47, 671–679.

Červený, V., Pšenčík, I., 1983. D Seismic Ray Tracing Package SEIS83 (Software Package). Charles University, Prague.

Cymerman, Z., Piasecki, M.A., Seston, R., 1997. Terranes and terrane boundaries in the Sudetes, northern Bohemian Massif. Geol. Mag. 134, 717–725.

Franke, W., 2000. The Mid-European segment of the Variscides: tectono–stratigraphic units, terrane bounadaries and plate tectonic evolution. Geol. Soc. London Spec. Publ. 179, 35–62.

Franke, W., Żelaźniewicz, A., 2002. Structure and evolution of the Bohemian Arc. Geol. Soc. London Spec. Publ. 201, 279–293.

Geissler, W.H., Kind, R., Kämpf, H., Klinge, K., Plenefisch, T., Zedník, J., W-BOHEMIA Working Group, 2002. Local Moho updoming beneath the western Eger Rift, Central Europe? Results from teleseismic receiver function. Geophys. Res. Abstr. 4 EGS-A-02297.

Grad, M., 1991. Seismic wave velocities in the sedimentary cover of the Palaeozoic Platform in Poland. Bull. Pol. Acad. Sci., Earth Sci. 39 (1), 13–22.

Grad, M., Trung Doan, T., Klimkowski, W., 1991. Seismic models of sedimentary cover of the Precambrian and Palaeozoic platforms in Poland. Publ. Inst. Geophys. Pol. Acad. Sc. A-19 (236), 125–145.

Grad, M., Keller, G.R., Thybo, H., Guterch, A., POLONAISE Working Group, 2002a. Lower lithospheric structure beneath the Trans-European Suture Zone from POLONAISE'97 seismic profiles. Tectonophysics 360, 153–168.

Grad, M., Guterch, A., Mazur, S., 2002b. Seismic refraction evidence for crustal structure in the central part of the Trans-European Suture Zone in Poland. In: Winchester, J.A., Pharaoh, T.C., Verniers, J. (Eds.), Palaeozoic Amalgamation of Central Europe, Geol. Soc. Spec. Publ. vol. 201, pp. 295–309.

Grad, M., Jensen, S.L., Keller, G.R., Guterch, A., Thybo, H., Janik, T., Tiira, T., Yliniemi, J., Luosto, U., Motuza, G., Nasedkin, V., Czuba, W., Gaczyński, E., Środa, P., Miller, K.C., Wilde-Piórko, M., Komminaho, K., Jacyna, J., Korabliova, L., 2003a. Crustal structure of the Trans-European suture zone region along POLONAISE'97 seismic profile P4. J. Geophys. Res. 108 (B11), 2541. doi:10.1029/2003JB002426.

Grad, M., Špičák, A., Keller, G.R., Guterch, A., Brož, M., Hegedűs, E., Working Group, 2003b. SUDETES 2003 seismic experiment. Stud. Geophys. Geod. 47, 681–689.

Grad, M., Guterch, A., Keller, G.R., Janik, T., Hegedűs, E., Vozár, J., Ślączka, A., Tiira, T., Yliniemi, J., CELEBRATION 2000 Working Group, in press. Lithospheric structure beneath trans-Carpathian transect from Precambrian platform to Pannonian basin—CELEBRATION 2000 seismic profile CEL05. J. Geophys. Res.

Grad, M., Guterch, A., Polkowska-Purys, A., 2005. Crustal structure of the Trans-European Suture Zone in central Poland — reinterpretation of LT-2, LT-4 and LT-5 deep seismic sounding profiles. Geol. Q. 49 (3), 243–252.

Guterch, A., Grad, M., Materzok, R., Perchuć, E., 1986. Deep structure of the Earth's crust in the contact zone of the Palaeozoic and Precambrian platforms in Poland (Tornquist–Teisseyre Zone). Tectonophysics 128, 251–279.

Guterch, A., Grad, M., Materzok, R., Perchuć, E., Janik, T., Gaczyński, E., Doan, T.T., Białek, T., Gadomski, D., Młynarski, S., Toporkiewicz, S., 1992. Laminated structure of the lower crust in the fore-Sudetic region in Poland, derived from seismic data. Phys. Earth Planet. Inter. 69, 217–223.

Guterch, A., Grad, M., Thybo, H., Keller, G.R., Miller, K., 1998. Seismic experiment spreads across Poland. Eos, Trans. Am. Geophys. Union 79 (26), 302–305.

Guterch, A., Grad, M., Thybo, H., Keller, G.R., POLONAISE Working Group, 1999. POLONAISE'97— international seismic experiment between Precambrian and Variscan Europe in Poland. Tectonophysics 314, 101–121.

Guterch, A., Grad, M., Keller, G.R., CELEBRATION 2000 Organizing Committee, 2001. Seismologists Celebrate The New Millenium with an Experiment in Central Europe. Eos, Transactions, American Geophysical Union 82 (45), 529, 534–535.

Guterch, A., Grad, M., Špičák, A., Brueckl, E., Hegedűs, E., Keller, G.R., CELEBRATION 2000, ALP 2002, SUDETES 2003 Working Groups, 2003a. An overview of recent seismic refraction experiments in Central Europe. Stud. Geophys. Geod. 47, 651–657.

Guterch, A., Grad, M., Keller, G.R., Posgay, K., Vozár, J., Špičák, A., Brueckl, E., Hajnal, Z., Thybo, H., CELEBRATION 2000 Experiment Team, 2003b. CELEBRATION 2000 seismic experiment. Stud. Geophys. Geod. 47, 659–669.

Hobro, J.W.D., 1999. Three-dimensional tomographic inversion of combined reflection and refraction seismic travel-time data. Ph.D. Thesis, Department of Earth Sciences, University of Cambridge.

Hole, J.R., 1992. Non-linear high resolution three-dimensional seismic travel time tomography. J. Geophys. Res. 97, 6553–6562.

Hrubcová, P., Środa, P., Špičák, A., Guterch, A., Grad, M., Keller, G.R., Brueckl, E., Thybo, H., 2005. Crustal and uppermost mantle structure of the Bohemian Massif based on CELEBRATION 2000 data. J. Geophys. Res. 110, B11305. doi:10.1029/2004JB003080.

Kind, R., Kosarev, G.L., Petersen, N.V., 1995. Receiver functions at the stations of the German Regional Seismic Network (GRSN). Geophys. J. Int. 121, 191–202.

Komminaho, K., 1998. Software manual for programs MODEL and XRAYS—a graphical interface for SEIS83 program package. Rep. 20, 31 pp. Dept. of Geophys., Univ. of Oulu, Finland.

Kozlovskaya, E., Janik, T., Yliniemi, J., Karatayev, G., Grad, M., 2004. Density–velocity relationship in the upper lithosphere obtained from P- and S-wave velocity models along the EUROBRIDGE'97 seismic profile and gravity data. Acta Geophys. Pol. 52 (4), 397–424.

Majdański, M., Grad, M., 2005. Application of second arrivals in seismic tomography inversion for the crustal structure study. Acta Geophys. Pol. 53 (1), 13–26.

Matte, Ph., Maluski, H., Rajlih, P., Franke, W., 1990. Terrane boundaries in the Bohemian Massif: result of large-scale Variscan shearing. Tectonophysics 177, 151–170.

Mayerová, M., Novotný, M., Fejfar, M., 1994. Deep seismic sounding in Czechoslovakia. In: Bucha, V., Bližkovský, M. (Eds.), Crustal Structure of the Bohemian Massif and West Carpathians. Academia Praha, pp. 13–21.

Neunhöfer, H., Marillier, F., Panza, G.F., 1981. Crust and upper mantle structure in the Bohemian Massif from the dispersion of Rayleigh waves. Gerlands Beitr. Geophys. 90, 514–520.

Novotný, O., Proskuryakova, T.S., Shilov, A.V., 1995. Dispersion of Rayleigh waves along the Prague–Warsaw profile. Stud. Geophys. Geod. 39, 138–147.

Novotný, O., Grad, M., Lund, C.-E., Urban, L., 1997. Verification of the lithospheric structure along profile Uppsala–Prague using surface wave dispersion. Stud. Geophys. Geod. 41, 15–28.

Paris, F., Robardet, M., 1990. Early Palaeozoic palaeobiogeography of the Variscan regions. Tectonophysics 177, 193–213.

Pin, C., 1990. Variscan oceans: ages, origins and geodynamic implications inferred from geochemical and radiometric data. Tectonophysics 177, 215–227.

Růžek, B., Vavryčuk, V., Hrubcová, P., Zedník, J., The CELEBRATION Working Group, 2003. Crustal anisotropy in the Bohemian Massif, Czech Republic: observations based on central European lithospheric experiment based on refraction (CELEBRATION) 2000. J. Geophys. Res. 108 (B8), 2392. doi:10.1029/2002JB002242.

Środa, P., 1999. Modifications of software package ZPLOT by C. Zelt. Inst. Geophys. Pol. Acad. Sc, Warsaw.

Środa, P., Czuba, W., Grad, M., Gaczyński, E., Guterch, A., 2002. Three-dimensional seismic modelling of crustal structure in the TESZ region based on POLONAISE '97 data. Tectonophysics 360, 169–185.

Tait, J., Schätz, M., Bachtadse, V., Soffel, H.C., 2000. Palaeomagnetism and Palaeozoic palaeogeography of Gondwana and European terranes. Geol. Soc. London Spec. Publ. 179, 21–34.

Unrug, R., Harańczyk, C., Chocyk-Jamińska, M., 1999. Easternmost Avalonian and Armorican–Cadomian terranes of central Europe and Caledonian–Variscan evolution of the polydeformed Kraków mobile belt geological constraints. Tectonophysics 302, 133–157.

Vavryčuk, V., Hrubcová, P., Brož, M., Málek, J., The ALP 2002 Working Group, 2004. Azimuthal variation of P_g velocity in the Moldanubian, Czech Republic: observations based on multi-azimuthal common-shot experiment. Tectonophysics 387, 189–203.

Wieland, E., Sigg, A., Plešinger, A., Horálek, J., 1987a. Deep structure of the Bohemian Massif from phase velocities of Rayleigh and Love waves. Phys. Earth Planet. Inter. 51, 155–156.

Wieland, E., Sigg, A., Plešinger, A., Horálek, J., 1987b. Deep structure of the Bohemian Massif from phase velocities of Rayleigh and Love waves. Stud. Geophys. Geod. 31, 1–7.

Wilde-Piórko, M., Saul, J., Grad, M., 2005. Differences in the crustal and uppermost mantle structures of the Bohemian Massif from teleseismic receiver functions. Stud. Geophys. Geod. 49, 85–107.

Winchester, J.A., The PACE TMR Network Team, 2002a. Palaeozoic amalgamation of Central Europe: new results from recent geological and geophysical investigations. Tectonophysics 360, 5–21.

Winchester, J.A., Pharaoh, T.C., Verniers, J., 2002b. Palaeozoic amalgamation of Central Europe: an introduction and synthesis of new results from recent geological and geophysical investigations. Geol. Soc. London Spec. Publ. 201, 1–18.

Żelaźniewicz, A., 1997. The Sudetes as a Palaeozoic orogen in central Europe. Geol. Mag. 134, 691–702.

Zelt, C.A., 1994. ZPLOT—an interactive plotting and picking program for seismic data. Bullard Lab., University of Cambridge, Cambridge UK.